applied optics

Fourier lightfield microscopy: a practical design guide

Laura Galdón,[1] Genaro Saavedra,[1] Jorge Garcia-Sucerquia,[1,2] Manuel Martínez-Corral,[1] and Emilio Sánchez-Ortiga[1,*]

[1]3D Imaging and Display Laboratory, Department of Optics, University of Valencia, E46100, Burjassot, Spain
[2]Universidad Nacional de Colombia Sede Medellín, School of Physics, A.A: 3840-Medellín-050034, Colombia
*Corresponding author: emilio.sanchez@uv.es

Received 18 January 2022; revised 23 February 2022; accepted 23 February 2022; posted 28 February 2022; published 21 March 2022

In this work, a practical guide for the design of a Fourier lightfield microscope is reported. The fundamentals of the Fourier lightfield are presented and condensed on a set of contour plots from which the user can select the design values of the spatial resolution, the field of view, and the depth of field, as function of the specifications of the hardware of the host microscope. This work guides the reader to select the parameters of the infinity-corrected microscope objective, the optical relay lenses, the aperture stop, the microlens array, and the digital camera. A user-friendly graphic calculator is included to ease the design, even to those who are not familiar with the lightfield technology. The guide is aimed to simplify the design process of a Fourier lightfield microscope, which sometimes could be a daunting task, and in this way, to invite the widespread use of this technology. An example of a design and experimental results on imaging different types of samples is also presented.

https://doi.org/10.1364/AO.453723

1. INTRODUCTION

Conventional microscopes have the ability of capturing 2D images of small specimen with high magnification and, above all, high spatial resolution. This unique feature is determined mainly by the numerical aperture (NA) of the microscope objective (MO). The main drawback of conventional microscopes is their poor performance for imaging 3D structures. This lack is caused, in part, by the fact that any pixel of the sensor, placed at the image plane, integrates the radiances of all the rays impinging on it. As consequence, the angular information of light emitted by the sample is lost. This drawback is often managed by making use of other feature of conventional microscopes: their short depth of field (DOF). This permits the capture of stacks of 2D images, focused at different depths, and from them to compute the 3D image. The main disadvantage of this later way of proceeding is the need for an axial scanning that increments substantially the recording time, which makes it useless in the case of dynamic specimen.

In this context, in the past few years lightfield microscopy (LFM) has been proposed as a powerful alternative regarding the recovery of 3D information of samples in a high-speed regime. As a result of its inherent capability of recovering spatial-angular information of a sample in a single shot without the need for an axial scanning, LFM is specially targeted to study the 3D behavior of rapid biological processes expressing relevant information in a given sample volume [1–5].

Based on the original idea proposed by Lippmann in 1908, under the name of integral photography [6], Levoy *et al.* reported the LFM concept [7,8]. In few words, they proposed to insert a microlens array (MLA) at the image plane of a conventional microscope and to set the sensor at the microlens rear focal plane. In practical terms, the implementation of LFM is not that simple since the NA of the microlenses should equal the NA of the objective, as evaluated at the image space. This means that, in fact, using a different objective lens from the objective revolver would imply the use of a different MLA.

The images captured by the LFM are composed by a collection of microimages, one per microlens, which store the spatial-angular information of the sample. A feature of LFM is that the perspective images, also named as elemental images (EIs), are not obtained directly but are computed from the microimages. The lateral resolution of EIs is determined by the microlens pitch, whereas the number of pixels covered by any microlens determines the density of the angular sampling. As a consequence, LFM provides images with a spatial resolution that is about 10 times worse that than of the host microscope where the MLA is inserted. Another drawback is the inhomogeneous lateral resolution of computed depth sections. Naturally, much work has been reported aiming to overcome these drawbacks by means of computational approaches. However, such methods have to tackle two essential difficulties. One is that the images captured by LFM have low spatial resolution; therefore, much high-frequency information has not been gathered and is, hence, impossible to be recovered by digital processing. The other is that, essentially, LFM images are not shift invariant; therefore, deconvolution procedures

cannot be applied directly. This implies that the algorithms to manipulate these images need to be highly sophisticated and time-consuming. Nevertheless, the results obtained by such computational methods are highly inspiring [9–11].

To overcome these drawbacks, Fourier lightfield microscopy (FLMic) was proposed [12–16]. FLMic is based in a new paradigm since the microlenses, whose pitch is now 1 order of magnitude bigger than in LFM, are placed no longer at the image plane but at its far field: the Fourier plane. Then the EIs are captured directly and have a spatial resolution that is just 3 to 5 times worse than that of the host microscope. Importantly, here the captured EIs have shift invariance, which allows the direct use of deconvolution tools and the computing of depth sections that have homogeneous resolution through the system DOF. An additional advantage of FLMic is that it can be implemented easily by inserting an accessory at the camera port of a regular commercial microscope and, therefore, can make use of the usual built-in features of the host microscope like, for example, the dark-field illumination mode [17,18].

Despite the great interest raised in the scientific and technological community [19–28], the widespread use of FLMic is yet limited. One of the factors that limits its use is that the design of these microscopes seems to be reserved to highly skilled teams in lightfield technology. To demystify the design of Fourier lightfield microscopes, this laboratory note presents a comprehensive guide including the basis of the FLMic technology, a design workflow that includes a graphical calculator of the hardware parameters, and a set of results to validate an example of design.

2. DESIGN FUNDAMENTALS

The setup of a regular FLMic is based on the use of an infinity-corrected MO, with given NA and magnification, a pair of relay lenses (with focal lengths f_1 an f_2) to have optical access to the aperture stop (AS) of the MO, an MLA, and a digital camera [13]. The two relay lenses are coupled in afocal manner, and at their common focal plane a field stop (FS) is placed, whose diameter is chosen to avoid any overlapping between the EIs. The digital camera is precisely located at the rear focal plane of the MLA. The latter is placed in the conjugate plane of the MO AS; this plane conjugation is done by the optical relay lenses. The sample is placed at the front focal plane of the infinity-corrected MO. In this way, several perspectives of the sample are generated in the plane of the digital sensor.

The FLMic produces as many views of the sample as microlenses are allocated in the conjugate AS. Further details of the design and operation of the FLMic can be read elsewhere [13–15]. A scheme of the proposed FLMic setup is shown in Fig. 1.

The implementation of an FLMic can be a challenging task especially for those not trained in lightfield imaging, due to the number of interlinked equations that determine the overall performance. For this reason, this laboratory note is aimed to provide a complete and intuitive guide for the design of an FLMic, supported on a graphical approach as well as a specifically designed calculator.

The design of an FLMic is based on a set of equations and procedures that describe the underlaying imaging process that takes place when recording the EIs. The lightfield is directly

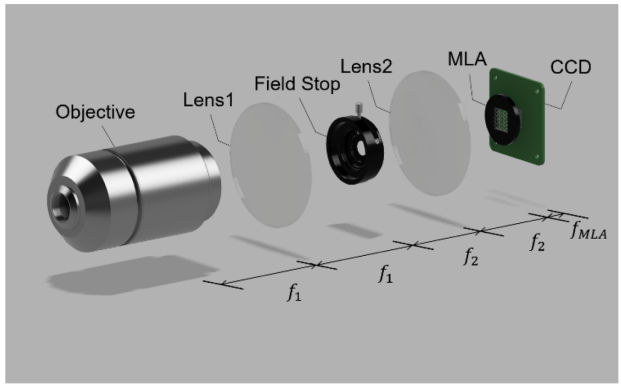

Fig. 1. Schematic drawing of an FLMic. f_1 and f_2 are the focal lengths of the relay lenses, and f_{MLA} is the focal length of the microlens array.

recorded by means of the sampling that the MLA does of the spatial-angular information at the far field located at the AS of the MO. In any regular infinity-corrected MO, its AS is not mechanically accessible; hence, it can be made optically accessible by means of the optical relay lenses that conjugate the AS plane with the plane of the MLA. This initial condition allows the calculation of the number of EIs to be recorded in a row, N, namely the number of microlenses that are fitted into the diameter of the AS, ϕ_{AS}:

$$N = \frac{\phi_{\mathrm{AS}}}{P} M_R, \tag{1}$$

with P being the pitch of the MLA and $M_R = f_2/f_1$ being the magnification of the relay system. The number N should be a number larger than 3, in order to have enough EIs to compute the depth sections; but it has also to be considered that the larger N is, the larger the resolution limit is and then the worse the resolution power of the microscope is. Note that the resolution power, which is often expressed in line pairs per millimeter (lp/mm), is just the inverse value of the resolution limit, which is usually expressed in micrometers (μm). The sampling of the AS done by the MLA means a reduction of the effective NA of the microscope, with the corresponding reduction of its resolution power. It has been studied that keeping N in the range from 3–5, the performance of the FLMic holds a right trade-off between reconstruction planes and resolution power penalization.

Usually, MO manufacturers do not provide the value of ϕ_{AS}, but it can be computed from the NA,

$$\phi_{\mathrm{AS}} = 2\ \tan(\arcsin(\mathrm{NA}))\ f_{\mathrm{MO}}. \tag{2}$$

It should be known that the focal length of an MO, f_{MO}, is neither provided. Instead, the manufacturer specifies the lateral magnification produced by the system composed of the MO and a tube lens (TL). The focal length of the MO is calculated as $f_{\mathrm{MO}} = f_{\mathrm{TL}}/M$, where M is the magnification marked on the MO barrel. Each manufacturer uses a different f_{TL}, typically between 160 and 200 mm. Therefore, to know f_{MO} of a given MO, it is mandatory to know the specifications provided by the manufacturer.

Conjugation relations are key in the FLMic design. One example is the FS, which is conjugated with the object plane and with the digital sensor. The size of the FS is set to avoid any

overlapping of the EIs while optimizing the use of the sensing area of the digital camera, but it subsequently determines the field of view (FOV) of the FLMic. The relating equations are

$$\phi_{\mathrm{FS}} = P\frac{f_2}{f_{\mathrm{MLA}}} \tag{3}$$

and

$$\mathrm{FOV} = \frac{P}{M_T}, \tag{4}$$

where

$$M_T = \frac{f_{\mathrm{MLA}}}{f_{\mathrm{MO}}}\frac{f_1}{f_2} \tag{5}$$

is the total magnification of the optical system.

The resolution limit of the directly captured EIs, strictly understood as the capability of resolving two incoherent light points separated a distance ρ_{EI} in the object plane, is given by combination of the diffractive ρ_{DIF} and geometric ρ_{GEO} resolution limits through:

$$\rho_{\mathrm{EI}} = \rho_{\mathrm{DIF}} + \rho_{\mathrm{GEO}} = N\frac{\lambda}{2\,\mathrm{NA}} + 2\frac{\delta}{M_T}, \tag{6}$$

with λ the illuminating wavelength and δ the pixel size. While ρ_{DIF} corresponds to the diffractive spatial resolution limit following Abbe's criterion [29], ρ_{GEO} accounts for the fulfilling of the Nyquist's criterion, which states that two separate object points are resolved if their images are captured by two different pixels, having at least one pixel between them [30]. Equation (6) expresses in the spatial domain the classical concepts reported by Boreman [31] and by Park *et al*. [32] in the frequency domain.

The final parameter to be considered is the DOF, which also is the result of the entanglement of the diffractive and the geometrical performance of FLMic. Accordingly, the DOF can be expressed as

$$\mathrm{DOF} = 2\lambda\frac{N^2}{\mathrm{NA}^2} + \frac{\delta}{M_T}\frac{N}{\mathrm{NA}}. \tag{7}$$

3. DESIGN WORKFLOW

The design of an FLMic must be guided by optimizing its hallmark of generating multiple views of a 3D sample via a single-shot recording. This single-shot approach allows the real-time imaging of 3D microscopic events. The price paid for this unique feature is the existence of a strong trade-off between the number of recorded views and the spatial resolution of the microscope [see Eq. (6)]. As consequence, an adequate starting point in the workflow design is the study of the spatial resolution as it changes in terms of the parameters that controls it.

Hardware-wise, an appropriate first point on the design process is to select the NA of the infinity-corrected MO. Without lack of generality and only for illustration purposes, an NA = 0.5, for which different manufactures offer varied set of focal lengths, is chosen here. The second step that can be taken is the selection of illumination light. Keeping in mind the possibility of using regular microscopy illumination systems, a $\lambda = 550$ nm has been chosen as the central wavelength of the white light impinging the sample. Another constraining parameter is the digital camera. Fortunately, one can find in the market very competitive cameras with a large variety of prices and specifications. For this example of design, a digital camera with a square pixel of side $\delta = 2.2$ μm is selected. The set of parameters selected in this paragraph, NA, λ, and δ, is what the designer must keep fixed to tune the focal lengths of the MO and MLA, and the pitch of the latter.

In Fig. 2, contour plots of the spatial resolution limit ρ_{EI}, whose values are represented according with the color scale, in terms of the focal lengths of the MO and the MLA are shown; each panel corresponds to a particular pitch of the MLA. Note that the slope of contour plots decreases toward the right side of the plots, where the diffractive contribution dominates over the geometrical one. From Eqs. (1) and (2), the number N of microlenses fitted within the AS of the MO varies with f_{MO}, with the focal lengths of the optical relay lenses, and with the pitch, P, of the MLA. It means that, for the given NA, the change of the said variables has to be controlled to keep N within the valid range for FLMic to work properly [13]; namely, it must range from 3 to 5.

For this design example, the equality $f_2 = f_1/2$ has been chosen for the sake of simplicity. In the contour plots of Fig. 2, horizontal white lines correspond to integer values of N so that the user can identify the recommended region given by $3 < N < 5$. The panels show that the minimum resolution limit that is theoretically achievable with the parameters that have been fixed is around $\rho_{EI} = 2.4$ μm in the case of $P = 0.8$ mm and $\rho_{\mathrm{EI}} = 3.0$ μm for $P = 1.4$ mm, for the smallest recommended number of EIs in a row, $N = 3$.

The study of the FOV and the DOF follows a similar procedure. The equations governing these features, Eqs. (4) and (7), respectively, have been used to produce the contour plots presented in Figs. 3 and 4. Again, the FLMic performance is

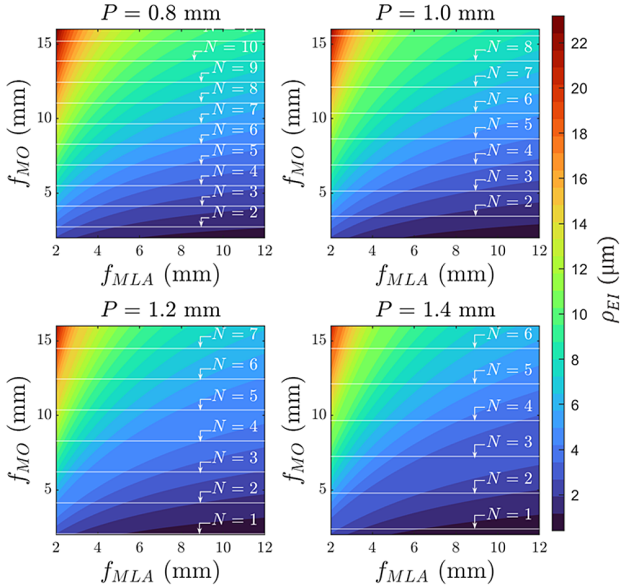

Fig. 2. Contour plots for the lateral resolution of the FLMic as the focal lengths of the MO and the MLA vary continuously and for different values of the MLA pitch. These plots are for the given values of NA = 0. 5, $\lambda = 550$ nm, $\delta = 2.2$ μm, and $f_1 = 2f_2$.

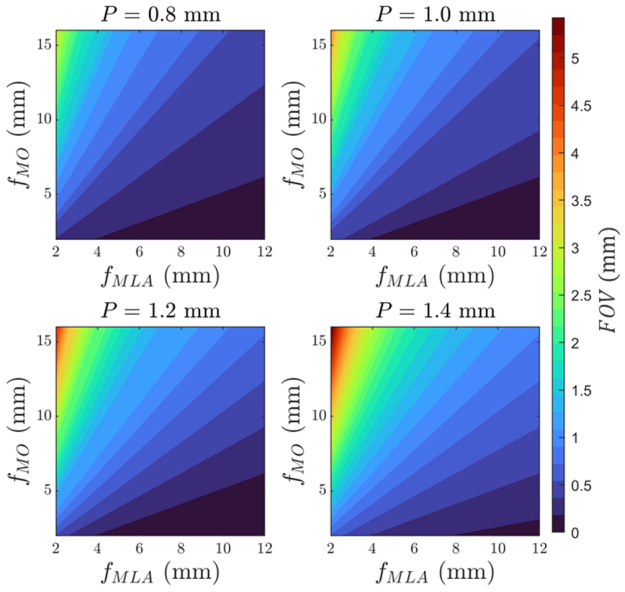

Fig. 3. Contour plots of the FOV for the same cases as in Fig. 2.

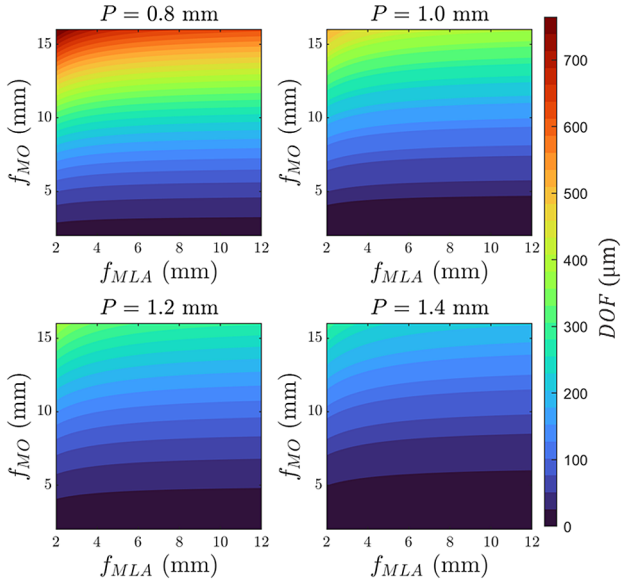

Fig. 4. Contour plots of the DOF for the same cases as in Fig. 2.

studied for continuously varying values of f_{MO} and f_{MLA} and for stepped values of P.

These contour plots show the possibility of obtaining FOVs ranging from approximately 0.1 to 5.4 mm in diameter, and DOFs in the range from 10 to 750 μm.

The contour plots shown in the workflow design can be combined to choose the hardware of a given FLMic. Without lack of generality, in the next example, an MLA has been selected with $P = 1$ mm, and again NA = 0.5, $f_2 = f_1/2$, and $\delta = 2.2$ μm. In Fig. 5, the contour plots for spatial resolution limit, FOV, and DOF have been arranged. These panels show the reachable values and allow the designer to choose which feature of the microscope to prioritize. If, for example, one has in stock a 40×/0.5 MO from Nikon (manufacturer that uses $f_{TL} = 200$ mm), it results in $N = 2.9$. Since this value is smaller

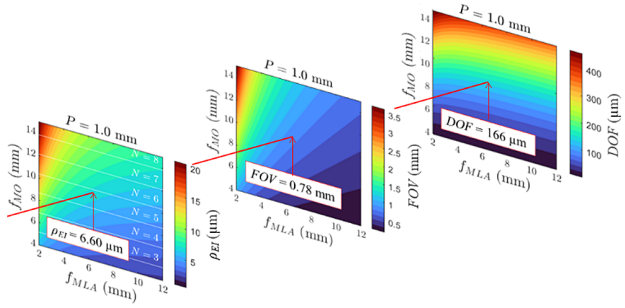

Fig. 5. Operational parameters of the designed hardware for this example of design.

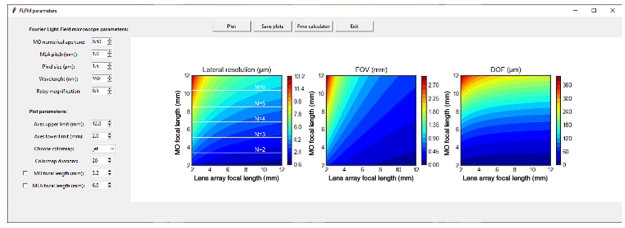

Fig. 6. Graphic calculator of the design parameters of FLMic.

than 3.0, it is convenient to try with other objective, or alternatively to modify the relay or the microlenses pitch. As a second trial example, 20×/0.5 Nikon MO and microlenses with $f_{MLA} = 6.43$ mm are chosen. In this case, $f_{MO} = 10$ mm, and the predicted values for the resulting FLMic are $\rho_{EI} = 6.60$ μm, FOV = 0.78 mm, and DOF = 166 μm.

As shown in Fig. 5, by drawing a straight line that intersects the three contour plots, the designer can pick the values of the optical features of the FLMic in a direct way.

To ease even further the design process, a self-contained and intuitive graphic calculator of the set of equations that governs the performance of FLMic has been developed within this work. The calculator was developed in Python and allows the user to define all the parameters that determine the lateral resolution, FOV, and DOF of the FLMic. In Fig. 6, a picture of its home screen is shown. Once these parameters are set, the graphic user interface (GUI) displays the three corresponding contour plots, like the ones shown in this manuscript. Furthermore, the user can set up the aspect of the contour plots by modifying the plotting region and the colormap, as well as the number of colormap divisions. In addition, to ease the reading of the values of each operational parameter of the FLMic, perpendicular dotted lines are displayed whose intersecting point indicates the computed value. Finally, the GUI includes an MO focal length calculator that only requires two inputs: the brand name and the magnification printed in the MO barrel. The calculator is available in Code 1, Ref. [33].

4. RESULTS

The example FLMic has been built and tested to validate its optical performance and contrast its figures with those forecasted by the design guide here presented. Then, an infinity-corrected MO 20×/0.5, with $f_{MO} = 10.0$ mm, coupled with an optical relay composed by two lenses of $f_1 = 200$ mm and

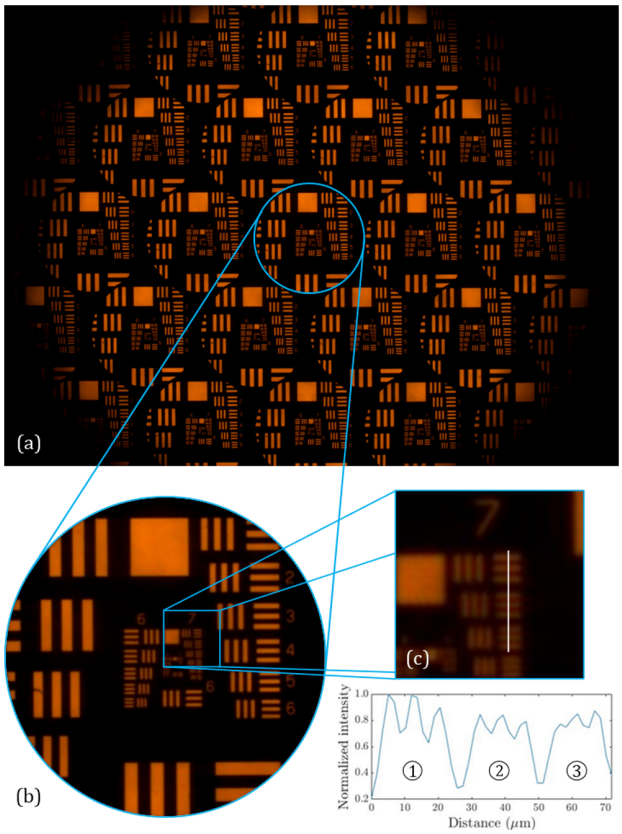

Fig. 7. Spatial resolution for the designed FLMic. (a) Complete set of recorded EIs. (b) Zoomed-in central EI. (c) Extra zoom corresponding to elements 1 to 3 of group 7. The plot profile along the white line shows that element 2 is resolved with contrast bigger than 10%.

$f_2 = 100$ mm, an MLA with $f_{\mathrm{MLA}} = 6.43$ mm and $P = 1$ mm, and a digital camera with 2560×1920 square pixels with $\delta = 2.2$ μm, was used. The spatial resolution, FOV, and DOF have been measured by capturing the multiple images of an USAF 1951 test target. Figure 7(a) shows the set of EIs recorded. From this panel, the central EI is zoomed-in and shown in Fig. 7(b). The elements from 1 to 4 of group number 7 are shown in Fig. 7(c) with a plot profile along the white line. From this plot, the reader can verify that the reached spatial resolution is 6.96 μm, which corresponds to element 2 of group 7, for which the contrast is still bigger than 10%. Conversely, a FOV of 0.76 mm in diameter is also obtained. These figures match well the design values, which are 6.60 μm and 0.78 mm, in that order.

The DOF is understood as the axial distance between the planes where the resolution falls a factor $\sqrt{2}$ of the value measured at the best focal plane. To test the DOF, the test target was axially displaced, backward and forward, while the spatial resolution was measured. The obtained DOF is 180 μm, which agrees within the 8% with the design value, which is 166 μm. Figure 8 shows the recorded central EIs utilized to measure the DOF. While Fig. 8(a) is recoded −110 μm apart from the best focal plane image in Fig. 8(b), Fig. 8(c) is registered +70 μm from the latter image.

Once the optical performance of the built FLMic is evaluated, it is used to image a sample of a grasshopper leg. Figure 9(a) shows the set of EIs recorded by the FLMic; Fig. 9(b) displays the refocused images between $z = 0.0$ μm and $z = 68.8$ μm. Distance z is measured from the best focal plane. Positive values of z correspond to depths between that plane and the MO.

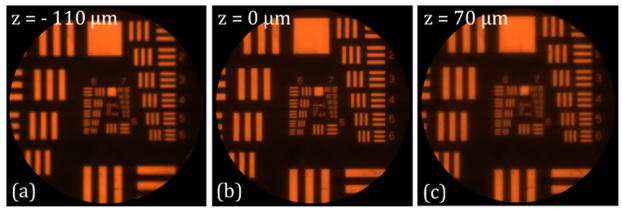

Fig. 8. Recorded central EIs at different depths to measure the DOF.

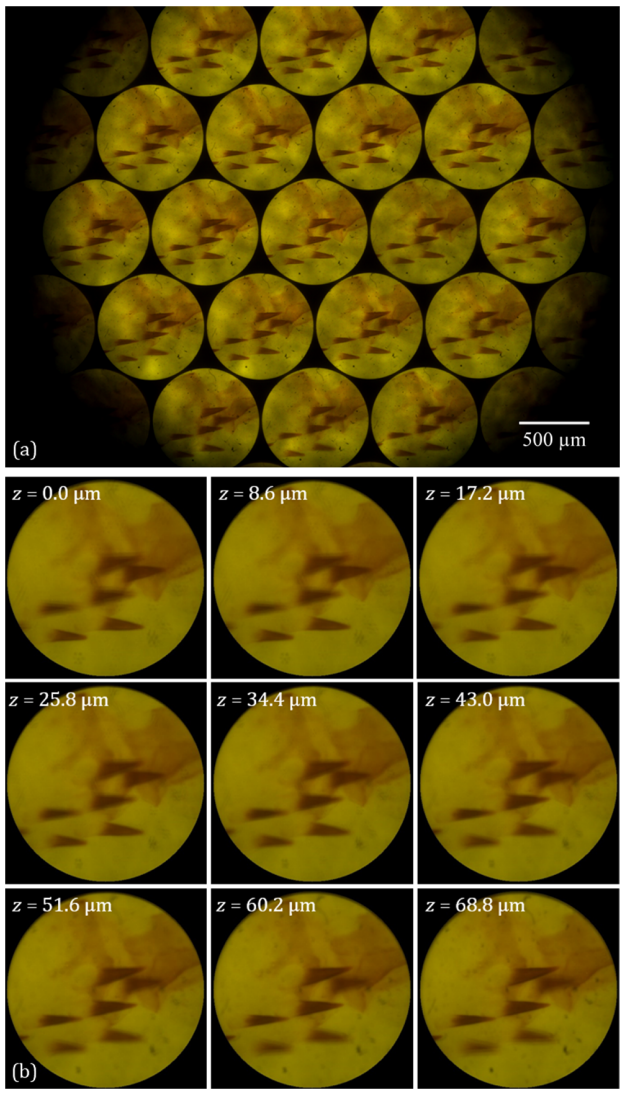

Fig. 9. (a) Elemental images of a grasshopper leg captured using the designed FLMic, indicating with a scale bar the distance in the object plane. Visualization 1 shows a movie built with the 7 central perspectives, i.e., the EIs. (b) Refocused images at different depth planes. Visualization 2 shows a movie whose frames are the refocused images.

5. CONCLUSION

Despite the progressive use of FLMic, the design process of this type of technology remains challenging. Even though the simple hardware needed to design and build an FLMic is composed of an infinity-corrected MO, an optical relay, an MLA, and a digital camera, the choice of their parameters to reach the wanted optical performance remains demanding. The entangled dependence of the spatial resolution, the FOV, and the DOF with the hardware specifications makes the design of FLMic a task almost exclusive of the skilled people in lightfield technology. As a contribution to ease the design process, in this laboratory note, there has been presented an intuitive and easy-to-use platform to attempt the design of an FLMic with a given optical performance.

The basis of FLMic has been recalled as establishing the essential framework within which the design is carried out, including additionally a graphical analysis of the governing equations. The design guide for the FLMic has been embedded in a user-friendly platform from which the designer can set the parameters of the needed hardware to obtain, both numerically and graphically, the computed values of the optical performance of the FLMic.

From an example of use, there has been designed and built an FLMic performing the optical features forecasted from the design stage. This example of application has been validated with experimental images of different types of samples.

Funding. Universidad Nacional de Colombia (Hermes 50069); Conselleria d'Educació, Cultura i Esport (PROMETEO/2019/048); Ministerio de Ciencia, Innovación y Universidades (RTI2018-099041-B-I00).

Acknowledgment. The authors thank Hui Yun for help with some drawings in this manuscript.

Disclosures. The authors declare no conflicts of interest.

Data availability. Data underlying the results presented in this paper are not publicly available at this time but may be obtained from the authors upon reasonable request.

REFERENCES

1. R. Prevedel, Y. G. Yoon, M. Hoffmann, N. Pak, G. Wetzstein, S. Kato, T. Schrödel, R. Raskar, M. Zimmer, E. S. Boyden, and A. Vaziri, "Simultaneous whole-animal 3D imaging of neuronal activity using light-field microscopy," Nat. Methods **11**, 727–730 (2014).
2. Y. Da Sie, C.-Y. Lin, and S.-J. Chen, "3D surface morphology imaging of opaque microstructures via light-field microscopy," Sci. Rep. **8**, 10505 (2018).
3. N. Wagner, N. Norlin, J. Gierten, G. de Medeiros, B. Balázs, J. Wittbrodt, L. Hufnagel, and R. Prevedel, "Instantaneous isotropic volumetric imaging of fast biological processes," Nat. Methods **16**, 497–500 (2019).
4. P. Quicke, C. L. Howe, P. Song, H. V. Jadan, C. Song, T. Knöpfel, M. Neil, P. L. Dragotti, S. R. Schultz, and A. J. Foust, "Subcellular resolution three-dimensional light-field imaging with genetically encoded voltage indicators," Neurophotonics **7**, 035006 (2020).
5. J. Wu, Z. Lu, D. Jiang, *et al.*, "Iterative tomography with digital adaptive optics permits hour-long intravital observation of 3D subcellular dynamics at millisecond scale," Cell **184**, 3318–3332 (2021).
6. G. Lippmann, "Epreuves reversibles donnant la sensation du relief," J. Phys. **7**, 821–825 (1908).
7. M. Levoy, R. Ng, A. Adams, M. Footer, and M. Horowitz, "Light field microscopy," ACM Trans. Graph. **25**, 924–934 (2006).
8. M. Levoy, Z. Zhang, and I. McDowall, "Recording and controlling the 4D light field in a microscope using microlens arrays," J. Microsc. **235**, 144–162 (2009).
9. A. Stefanoiu, J. Page, P. Symvoulidis, G. G. Westmeyer, and T. Lasser, "Artifact-free deconvolution in light field microscopy," Opt. Express **27**, 31644–31666 (2019).
10. Y. Zhang, Z. Lu, J. Wu, X. Lin, D. Jiang, Y. Cai, J. Xie, Y. Wang, T. Zhu, X. Ji, and Q. Dai, "Computational optical sectioning with an incoherent multiscale scattering model for light-field microscopy," Nat. Commun. **12**, 6391 (2021).
11. N. Wagner, F. Beuttenmueller, N. Norlin, J. Gierten, J. C. Boffi, J. Wittbrodt, M. Weigert, L. Hufnagel, R. Prevedel, and A. Kreshuk, "Deep learning-enhanced light-field imaging with continuous validation," Nat. Methods **18**, 557–563 (2021).
12. A. Llavador, J. Sola-Pikabea, G. Saavedra, B. Javidi, and M. Martinez-Corral, "Resolution improvements in integral microscopy with Fourier plane recording," Opt. Express **24**, 20792–20798 (2016).
13. G. Scrofani, J. Sola-Pikabea, A. Llavador, E. Sanchez-Ortiga, J. C. Barreiro, G. Saavedra, J. Garcia-Sucerquia, and M. Martinez-Corral, "FIMic: design for ultimate 3D-integral microscopy of in-vivo biological samples," Biomed. Opt. Express **9**, 335–346 (2018).
14. C. Guo, W. Liu, X. Hua, H. Li, and S. Jia, "Fourier light-field microscopy," Opt. Express **27**, 25573–25594 (2019).
15. E. Sanchez-Ortiga, G. Scrofani, G. Saavedra, and M. Martinez-Corral, "Optical sectioning microscopy through single-shot lightfield protocol," IEEE Access **8**, 14944–14952 (2020).
16. F. L. Liu, G. Kuo, N. Antipa, K. Yanny, and L. Waller, "Fourier DiffuserScope: single-shot 3D Fourier light field microscopy with a diffuser," Opt. Express **28**, 28969–28986 (2020).
17. N. Incardona, A. Tolosa, G. Scrofani, M. Martinez-Corral, and G. Saavedra, "The lightfield microscope eyepiece," Sensors **21**, 6619 (2021).
18. G. Scrofani, G. Saavedra, M. Martínez-Corral, and E. Sánchez-Ortiga, "Three-dimensional real-time darkfield imaging through Fourier lightfield microscopy," Opt. Express **28**, 30513–30519 (2020).
19. L. Cong, Z. Wang, Y. Chai, W. Hang, C. Shang, W. Yang, L. Bai, J. Du, K. Wang, and Q. Wen, "Rapid whole brain imaging of neural activity in freely behaving larval zebrafish (Danio rerio)," eLife **6**, e28158 (2017).
20. M. Martinez-Corral and B. Javidi, "Fundamentals of 3D imaging and displays: a tutorial on integral imaging, light-field, and plenoptic systems," Adv. Opt. Photon. **10**, 512–566 (2018).
21. Y. G. Yoon, Z. Wang, N. Pak, D. Park, P. Dai, J. S. Kang, H. J. Suk, P. Symvoulidis, B. Guner-Ataman, K. Wang, and E. S. Boyden, "Sparse decomposition light-field microscopy for high speed imaging of neuronal activity," Optica **7**, 1457–1468 (2020).
22. B. Javidi, A. Carnicer, J. Arai, T. Fujii, H. Hua, H. Liao, M. Martínez-Corral, F. Pla, A. Stern, L. Waller, Q.-H. Wang, G. Wetzstein, M. Yamaguchi, and H. Yamamoto, "Roadmap on 3D integral imaging: sensing, processing, and display," Opt. Express **28**, 32266–32293 (2020).
23. R. R. Sims, S. Abdul Rehman, M. O. Lenz, S. I. Benaissa, E. Bruggeman, A. Clark, E. W. Sanders, A. Ponjavic, L. Muresan, S. F. Lee, and K. O'Holleran, "Single molecule light field microscopy," Optica **7**, 1065–1072 (2020).
24. A. Stefanoiu, G. Scrofani, G. Saavedra, M. Martinez-Corral, and T. Lasser, "What about computational super-resolution in fluorescence Fourier light field microscopy?" Opt. Express **28**, 16554–16568 (2020).
25. K. Yanny, N. Antipa, W. Liberti, S. Dehaeck, K. Monakhova, F. Liu, K. Shen, R. Ng, and L. Waller, "Miniscope3D: optimized single-shot miniature 3D fluorescence microscopy," Light Sci. Appl. **9**, 171 (2020).
26. Q. Cui, J. Park, Y. Ma, and L. Gao, "Snapshot hyperspectral light field tomography," Optica **8**, 1552–1558 (2021).
27. X. Hua, W. Liu, and S. Jia, "High-resolution Fourier light-field microscopy for volumetric multi-color live-cell imaging," Optica **8**, 614–620 (2021).
28. Z. Wang, L. Zhu, H. Zhang, G. Li, C. Yi, Y. Yang, Y. Ding, M. Zhen, S. Gao, T. K. Hsiai, and P. Fei, "Real-time volumetric reconstruction of biological dynamics with light-field microscopy and deep learning," Nat. Methods **18**, 551–556 (2021).
29. M. Pluta, *Advanced Light Microscopy: Principles and Basic Properties* (Elsevier, 1988).
30. J. W. Goodman, *Introduction to Fourier Optics* (McGraw-Hill, 1996).

31. G. D. Boreman, *Modulation Transfer Function in Optical and Electro-Optical Systems* (SPIE, 2001).
32. S. K. Park, R. Schowengerdt, and M. A. Kaczynski, "Modulation-transfer-function analysis for sampled image systems," Appl. Opt. **23**, 2572–2582 (1984).
33. E. Sanchez-Ortiga, L. Galdón, J. Garcia-Sucerquia, M. Martinez-Corral, and G. Saavedra, "Fourier lightfield calculator," figshare (2022), https://doi.org/10.6084/m9.figshare.19213068.